DESY 96-046
March 1996

ISSN 0418-9833

Measurement of the Q^2 dependence of the Charged and Neutral Current Cross Sections in $e^{\pm}p$ Scattering at HERA

H1 Collaboration

Abstract:

The Q^2 dependence and the total cross sections for charged and neutral current processes are measured in $e^{\pm}p$ reactions for transverse momenta of the outgoing lepton larger than 25 GeV. Comparable size of cross sections for the neutral current process and for the weak charged current process are observed above $Q^2 \approx 5000$ GeV^2. Using the shape and magnitude of the charged current cross section we determine a propagator mass of $m_W = 84\ ^{+10}_{-7}$ GeV.

S. Aid[14], V. Andreev[26], B. Andrieu[29], R.-D. Appuhn[12], M. Arpagaus[37], A. Babaev[25], J. Bähr[36], J. Bán[18], Y. Ban[28], P. Baranov[26], E. Barrelet[30], R. Barschke[12], W. Bartel[12], M. Barth[5], U. Bassler[30], H.P. Beck[38], H.-J. Behrend[12], A. Belousov[26], Ch. Berger[1], G. Bernardi[30], R. Bernet[37], G. Bertrand-Coremans[5], M. Besançon[10], R. Beyer[12], P. Biddulph[23], P. Bispham[23], J.C. Bizot[28], V. Blobel[14], K. Borras[9], F. Botterweck[5], V. Boudry[29], A. Braemer[15], W. Braunschweig[1], V. Brisson[28], D. Bruncko[18], C. Brune[16], R. Buchholz[12], L. Büngener[14], J. Bürger[12], F.W. Büsser[14], A. Buniatian[12,39], S. Burke[19], M.J. Burton[23], G. Buschhorn[27], A.J. Campbell[12], T. Carli[27], M. Charlet[12], D. Clarke[6], A.B. Clegg[19], B. Clerbaux[5], S. Cocks[20], J.G. Contreras[9], C. Cormack[20], J.A. Coughlan[6], A. Courau[28], M.-C. Cousinou[24], G. Cozzika[10], L. Criegee[12], D.G. Cussans[6], J. Cvach[31], S. Dagoret[30], J.B. Dainton[20], W.D. Dau[17], K. Daum[35], M. David[10], C.L. Davis[19], B. Delcourt[28], A. De Roeck[12], E.A. De Wolf[5], M. Dirkmann[9], P. Dixon[19], P. Di Nezza[33], W. Dlugosz[8], C. Dollfus[38], J.D. Dowell[4], H.B. Dreis[2], A. Droutskoi[25], D. Düllmann[14], O. Dünger[14], H. Duhm[13], J. Ebert[35], T.R. Ebert[20], G. Eckerlin[12], V. Efremenko[25], S. Egli[38], R. Eichler[37], F. Eisele[15], E. Eisenhandler[21], R.J. Ellison[23], E. Elsen[12], M. Erdmann[15], W. Erdmann[37], E. Evrard[5], A.B. Fahr[14], L. Favart[28], A. Fedotov[25], D. Feeken[14], R. Felst[12], J. Feltesse[10], J. Ferencei[18], F. Ferrarotto[33], K. Flamm[12], M. Fleischer[9], M. Flieser[27], G. Flügge[2], A. Fomenko[26], B. Fominykh[25], J. Formánek[32], J.M. Foster[23], G. Franke[12], E. Fretwurst[13], E. Gabathuler[20], K. Gabathuler[34], F. Gaede[27], J. Garvey[4], J. Gayler[12], M. Gebauer[36], A. Gellrich[12], H. Genzel[1], R. Gerhards[12], A. Glazov[36], U. Goerlach[12], L. Goerlich[7], N. Gogitidze[26], M. Goldberg[30], D. Goldner[9], K. Golec-Biernat[7], B. Gonzalez-Pineiro[30], I. Gorelov[25], C. Grab[37], H. Grässler[2], R. Grässler[2], T. Greenshaw[20], R. Griffiths[21], G. Grindhammer[27], A. Gruber[27], C. Gruber[17], J. Haack[36], D. Haidt[12], L. Hajduk[7], M. Hampel[1], M. Hapke[12], W.J. Haynes[6], G. Heinzelmann[14], R.C.W. Henderson[19], H. Henschel[36], I. Herynek[31], M.F. Hess[27], W. Hildesheim[12], K.H. Hiller[36], C.D. Hilton[23], J. Hladký[31], K.C. Hoeger[23], M. Höppner[9], D. Hoffmann[12], T. Holtom[20], R. Horisberger[34], V.L. Hudgson[4], M. Hütte[9], H. Hufnagel[15], M. Ibbotson[23], H. Itterbeck[1], A. Jacholkowska[28], C. Jacobsson[22], M. Jaffre[28], J. Janoth[16], T. Jansen[12], L. Jönsson[22], K. Johannsen[14], D.P. Johnson[5], L. Johnson[19], H. Jung[10], P.I.P. Kalmus[21], M. Kander[12], D. Kant[21], R. Kaschowitz[2], U. Kathage[17], J. Katzy[15], H.H. Kaufmann[36], O. Kaufmann[15], S. Kazarian[12], I.R. Kenyon[4], S. Kermiche[24], C. Keuker[1], C. Kiesling[27], M. Klein[36], C. Kleinwort[12], G. Knies[12], T. Köhler[1], J.H. Köhne[27], H. Kolanoski[3], F. Kole[8], S.D. Kolya[23], V. Korbel[12], M. Korn[9], P. Kostka[36], S.K. Kotelnikov[26], T. Krämerkämper[9], M.W. Krasny[7,30], H. Krehbiel[12], D. Krücker[2], U. Krüger[12], U. Krüner-Marquis[12], H. Küster[22], M. Kuhlen[27], T. Kurča[36], J. Kurzhöfer[9], D. Lacour[30], B. Laforge[10], R. Lander[8], M.P.J. Landon[21], W. Lange[36], U. Langenegger[37], J.-F. Laporte[10], A. Lebedev[26], F. Lehner[12], C. Leverenz[12], S. Levonian[29], Ch. Ley[2], G. Lindström[13], M. Lindstroem[22], J. Link[8], F. Linsel[12], J. Lipinski[14], B. List[12], G. Lobo[28], H. Lohmander[22], J.W. Lomas[23], G.C. Lopez[13], V. Lubimov[25], D. Lüke[9,12], N. Magnussen[35], E. Malinovski[26], S. Mani[8], R. Maraček[18], P. Marage[5], J. Marks[24], R. Marshall[23], J. Martens[35], G. Martin[14], R. Martin[20], H.-U. Martyn[1], J. Martyniak[7], T. Mavroidis[21], S.J. Maxfield[20], S.J. McMahon[20], A. Mehta[6], K. Meier[16], T. Merz[36], A. Meyer[14], A. Meyer[12], H. Meyer[35], J. Meyer[12], P.-O. Meyer[2], A. Migliori[29], S. Mikocki[7], D. Milstead[20], J. Moeck[27], F. Moreau[29], J.V. Morris[6], E. Mroczko[7], D. Müller[38], G. Müller[12], K. Müller[12], P. Murín[18], V. Nagovizin[25], R. Nahnhauer[36], B. Naroska[14], Th. Naumann[36], P.R. Newman[4], D. Newton[19], D. Neyret[30], H.K. Nguyen[30], T.C. Nicholls[4], F. Niebergall[14], C. Niebuhr[12], Ch. Niedzballa[1], H. Niggli[37], R. Nisius[1], G. Nowak[7], G.W. Noyes[6], M. Nyberg-Werther[22], M. Oakden[20], H. Oberlack[27], U. Obrock[9], J.E. Olsson[12], D. Ozerov[25], P. Palmen[2], E. Panaro[12], A. Panitch[5], C. Pascaud[28], G.D. Patel[20], H. Pawletta[2], E. Peppel[36], E. Perez[10], J.P. Phillips[20], A. Pieuchot[24], D. Pitzl[37], G. Pope[8], S. Prell[12], R. Prosi[12], K. Rabbertz[1], G. Rädel[12], F. Raupach[1], P. Reimer[31], S. Reinshagen[12], H. Rick[9], V. Riech[13], J. Riedlberger[37], F. Riepenhausen[2], S. Riess[14], E. Rizvi[21], S.M. Robertson[4], P. Robmann[38], H.E. Roloff[† 36], R. Roosen[5], K. Rosenbauer[1], A. Rostovtsev[25], F. Rouse[8], C. Royon[10], K. Rüter[27], S. Rusakov[26], K. Rybicki[7], N. Sahlmann[2], D.P.C. Sankey[6], P. Schacht[27], S. Schiek[14], S. Schleif[16], P. Schleper[15], W. von Schlippe[21], D. Schmidt[35], G. Schmidt[14], A. Schöning[12], V. Schröder[12], E. Schuhmann[27], B. Schwab[15], F. Sefkow[12], M. Seidel[13], R. Sell[12], A. Semenov[25], V. Shekelyan[12], I. Sheviakov[26], L.N. Shtarkov[26], G. Siegmon[17], U. Siewert[17], Y. Sirois[29], I.O. Skillicorn[11], P. Smirnov[26], J.R. Smith[8], V. Solochenko[25], Y. Soloviev[26], A. Specka[29], J. Spiekermann[9], S. Spielman[29], H. Spitzer[14], F. Squinabol[28], R. Starosta[1], M. Steenbock[14], P. Steffen[12], R. Steinberg[2], H. Steiner[12,40], B. Stella[33], A. Stellberger[16], J. Stier[12], J. Stiewe[16], U. Stößlein[36], K. Stolze[36], U. Straumann[38], W. Struczinski[2], J.P. Sutton[4], S. Tapprogge[16], M. Taševský[32], V. Tchernyshov[25], S. Tchetchelnitski[25], J. Theissen[2], C. Thiebaux[29], G. Thompson[21], P. Truöl[38], J. Turnau[7], J. Tutas[15], P. Uelkes[2], A. Usik[26], S. Valkár[32], A. Valkárová[32], C. Vallée[24], D. Vandenplas[29], P. Van Esch[5], P. Van Mechelen[5], Y. Vazdik[26], P. Verrecchia[10], G. Villet[10], K. Wacker[9], A. Wagener[2], M. Wagener[34], A. Walther[9], B. Waugh[23], G. Weber[14], M. Weber[12], D. Wegener[9], A. Wegner[27], T. Wengler[15], M. Werner[15], L.R. West[4], T. Wilksen[12], S. Willard[8], M. Winde[36], G.-G. Winter[12], C. Wittek[14], E. Wünsch[12], J. Žáček[32], D. Zarbock[13], Z. Zhang[28], A. Zhokin[25], F. Zomer[28], J. Zsembery[10], K. Zuber[16], and M. zurNedden[38]

[1] I. Physikalisches Institut der RWTH, Aachen, Germany[a]
[2] III. Physikalisches Institut der RWTH, Aachen, Germany[a]
[3] Institut für Physik, Humboldt-Universität, Berlin, Germany[a]
[4] School of Physics and Space Research, University of Birmingham, Birmingham, UK[b]
[5] Inter-University Institute for High Energies ULB-VUB, Brussels; Universitaire Instelling Antwerpen, Wilrijk; Belgium[c]
[6] Rutherford Appleton Laboratory, Chilton, Didcot, UK[b]
[7] Institute for Nuclear Physics, Cracow, Poland[d]
[8] Physics Department and IIRPA, University of California, Davis, California, USA[e]
[9] Institut für Physik, Universität Dortmund, Dortmund, Germany[a]
[10] CEA, DSM/DAPNIA, CE-Saclay, Gif-sur-Yvette, France
[11] Department of Physics and Astronomy, University of Glasgow, Glasgow, UK[b]
[12] DESY, Hamburg, Germany[a]
[13] I. Institut für Experimentalphysik, Universität Hamburg, Hamburg, Germany[a]
[14] II. Institut für Experimentalphysik, Universität Hamburg, Hamburg, Germany[a]
[15] Physikalisches Institut, Universität Heidelberg, Heidelberg, Germany[a]
[16] Institut für Hochenergiephysik, Universität Heidelberg, Heidelberg, Germany[a]
[17] Institut für Reine und Angewandte Kernphysik, Universität Kiel, Kiel, Germany[a]
[18] Institute of Experimental Physics, Slovak Academy of Sciences, Košice, Slovak Republic[f]
[19] School of Physics and Chemistry, University of Lancaster, Lancaster, UK[b]
[20] Department of Physics, University of Liverpool, Liverpool, UK[b]
[21] Queen Mary and Westfield College, London, UK[b]
[22] Physics Department, University of Lund, Lund, Sweden[g]
[23] Physics Department, University of Manchester, Manchester, UK[b]
[24] CPPM, Université d'Aix-Marseille II, IN2P3-CNRS, Marseille, France
[25] Institute for Theoretical and Experimental Physics, Moscow, Russia
[26] Lebedev Physical Institute, Moscow, Russia[f]
[27] Max-Planck-Institut für Physik, München, Germany[a]
[28] LAL, Université de Paris-Sud, IN2P3-CNRS, Orsay, France
[29] LPNHE, Ecole Polytechnique, IN2P3-CNRS, Palaiseau, France
[30] LPNHE, Universités Paris VI and VII, IN2P3-CNRS, Paris, France
[31] Institute of Physics, Czech Academy of Sciences, Praha, Czech Republic[f,h]
[32] Nuclear Center, Charles University, Praha, Czech Republic[f,h]
[33] INFN Roma and Dipartimento di Fisica, Universita "La Sapienza", Roma, Italy
[34] Paul Scherrer Institut, Villigen, Switzerland
[35] Fachbereich Physik, Bergische Universität Gesamthochschule Wuppertal, Wuppertal, Germany[a]
[36] DESY, Institut für Hochenergiephysik, Zeuthen, Germany[a]
[37] Institut für Teilchenphysik, ETH, Zürich, Switzerland[i]
[38] Physik-Institut der Universität Zürich, Zürich, Switzerland[i]
[39] Visitor from Yerevan Phys. Inst., Armenia
[40] On leave from LBL, Berkeley, USA
† Deceased

[a] Supported by the Bundesministerium für Bildung, Wissenschaft, Forschung und Technologie, FRG, under contract numbers 6AC17P, 6AC47P, 6DO57I, 6HH17P, 6HH27I, 6HD17I, 6HD27I, 6KI17P, 6MP17I, and 6WT87P
[b] Supported by the UK Particle Physics and Astronomy Research Council, and formerly by the UK Science and Engineering Research Council
[c] Supported by FNRS-NFWO, IISN-IIKW
[d] Supported by the Polish State Committee for Scientific Research, grant nos. 115/E-743/SPUB/P03/109/95 and 2 P03B 244 08p01, and Stiftung für Deutsch-Polnische Zusammenarbeit, project no.506/92
[e] Supported in part by USDOE grant DE F603 91ER40674
[f] Supported by the Deutsche Forschungsgemeinschaft
[g] Supported by the Swedish Natural Science Research Council
[h] Supported by GA ČR, grant no. 202/93/2423, GA AV ČR, grant no. 19095 and GA UK, grant no. 342
[i] Supported by the Swiss National Science Foundation

1 Introduction

The unification of weak and electromagnetic forces is an important ingredient of the Standard Model. As a consequence the cross sections for neutral current (NC) and charged current (CC) processes

$$e^{\pm}p \to e^{\pm} + X \qquad \text{and} \qquad e^{\pm}p \to \overset{(-)}{\nu}_e + X \tag{1}$$

(X denotes the hadronic system recoiling against the lepton) are predicted to be of comparable size when probing small distances. The H1 experiment at the electron–proton collider HERA permits the study of these processes at large squared four momentum transfer Q^2 using the same detector for the measurement of both processes.

The generalized cross sections for deep–inelastic $e^{\pm}p$-scattering can be written as [1]:

$$\frac{\mathrm{d}^2\sigma(e^{\pm}p)}{\mathrm{d}x\mathrm{d}Q^2} = \frac{2\pi\alpha^2}{xQ^4}\left((1+(1-y)^2)\mathcal{F}_2 \mp (1-(1-y)^2)x\mathcal{F}_3\right). \tag{2}$$

Here x and y are the Bjorken scaling variables which are related by $Q^2 = sxy$. The center of mass energy squared s is given by the product of the electron and proton beam energies $s = 4E_eE_p$. The electromagnetic coupling constant is denoted α and $\mathcal{F}_{2,3}$ are generalized structure functions. These cross sections contain not only the proton structure functions but also the electroweak coupling constants and propagator terms. The contribution of the longitudinal structure function F_L is expected to be small at high Q^2 and is neglected here.

The NC cross section is governed by the photon propagator while the Z^0 exchange affects the cross sections significantly only at $Q^2 \approx m^2_{Z^0}$. Also the contribution of the Z^0 exchange enters with different signs for e^+p and e^-p scattering. The difference between the two NC cross sections therefore provides a method for detecting these electroweak effects. However, the accumulated statistics of the NC data are not yet sufficient to distinguish the dominant photon contribution from Z^0-exchange.

For CC processes the lowest order cross section can be simplified to

$$\frac{\mathrm{d}^2\sigma^{e^-p}_{\mathrm{CC}}}{\mathrm{d}x\mathrm{d}Q^2} = \frac{G^2_\mu}{2\pi}\frac{1}{(1+Q^2/m^2_W)^2}\left[\sum_{q=u,c} q(x,Q^2) + \sum_{\bar{q}=\bar{d},\bar{s},\bar{b}} (1-y)^2\bar{q}(x,Q^2)\right] \tag{3}$$

$$\frac{\mathrm{d}^2\sigma^{e^+p}_{\mathrm{CC}}}{\mathrm{d}x\mathrm{d}Q^2} = \frac{G^2_\mu}{2\pi}\frac{1}{(1+Q^2/m^2_W)^2}\left[\sum_{\bar{q}=\bar{u},\bar{c}} \bar{q}(x,Q^2) + \sum_{q=d,s,b} (1-y)^2 q(x,Q^2)\right] \tag{4}$$

where q and $\bar{q}$ are the quark and anti-quark densities of the proton. G_μ is the Fermi constant known from the measurement of the muon lifetime. In the propagator term m_W denotes the mass of the W bosons which mediate the weak force.

In our previous publications total charged current cross section measurements have been presented [2, 3]. In this analysis we study the dependence of the charged current cross section on the four momentum transfer. Such an analysis has been presented earlier by the ZEUS Collaboration [4] for 1993 e^-p. Here we present results obtained from both e^-p and e^+p data recorded in 1993 and 1994. From the cross section and the shape of the Q^2 distribution we derive m_W.

Neutral current cross sections at high Q^2 have already been precisely measured using the information provided by the scattered lepton only [5] or together with the hadronic final state [6]. For the comparison with charged current processes we use here the hadronic final state for event selection as well as for kinematic reconstruction. This procedure reduces uncertainties arising from different systematic effects.

2 Experimental conditions

HERA is an ep-collider where electron or positron beams collide with 820 GeV protons. This analysis is based on data taken in 1993 and 1994 using the H1 detector. The integrated luminosities are 0.33 pb^{-1} (1993) and 0.36 pb^{-1}(1994) for e^-p running and 2.70 pb^{-1}(1994) for e^+p running. The lepton beam energies were 26.7 GeV in 1993 and 27.5 GeV in 1994.

H1 is a multi–purpose detector well optimized to measure large Q^2 events in deep inelastic scattering. A detailed description of the H1 detector and its performance can be found in [7]. We discuss those aspects which are relevant to the present analysis.

A system of central and forward drift chambers is used to determine the interaction vertex of an event. The chambers measure tracks from charged particles in the polar angular range of $7^\circ - 165^\circ$ with respect to the proton beam direction (which is the $+z$-direction). The drift chambers are complemented by several layers of proportional chambers which provide fast trigger signals.

The energy and angles of the hadronic final state particles as well as the scattered electron are measured in the highly segmented (≈ 45000 cells) liquid argon (LAr) calorimeter [8]. It covers a polar angular range between 4° and 153°. The total depth of the calorimeter varies between 4.5 and 8 interaction lengths. The resolution for single pions and electrons is $\sigma(E)/E \approx 0.50/\sqrt{(E/\mathrm{GeV})} \oplus 0.02$ and $\sigma(E)/E \approx 0.11/\sqrt{(E/\mathrm{GeV})} \oplus 0.01$ respectively, as measured in test beam [9]. The hadron energy scale is verified within 4% with data taken at HERA [10]. For trigger purposes the LAr calorimeter is read out in a coarser granularity via flash ADCs. They provide a fast measurement of energies and allow triggering on missing transverse momenta (CC trigger) or on large electromagnetic energy deposition (NC trigger).

Both the LAr calorimeter and the central drift chambers are surrounded by a superconducting solenoid. The iron yoke which returns the magnetic flux is instrumented with streamer tubes and is used as a muon detector.

A luminosity system measures the rate of the small angle Bremsstrahlung process $ep \rightarrow ep\gamma$ [11] and allows the determination of the luminosity with a precision of 1.5% (3.5% in 1993).

3 Data Samples

The selection starts from all triggered events and is based on information of the hadronic final state both for CC and NC interactions. The presence or absence of a charged scattered lepton is used only to classify an event as a candidate for a CC or a NC process.

Scattered electrons are identified in the LAr calorimeter by the lateral extension and energy density of the electromagnetic shower and the requirement that a reconstructed track points to the shower. The minimal transverse energy deposition of the electron candidate is required to be 5 GeV [12]. The search is restricted to scattering angles of the charged lepton $\vartheta_e < 150^o$, which is well inside the angular acceptance of the liquid argon calorimeter. The efficiency of the electron identification is determined by comparing independent electron identification algorithms, either based on calorimeter information only or on a track criterion.

A total electron identification efficiency of $98.7 \pm 0.3\%$ is found for the finally analysed NC sample.

After the neutral current candidates are identified all information about the electron in the track detectors and calorimeters is ignored in the subsequent analysis. The additional selection described below is applied to both samples on the hadronic final state only. The selection steps are as follows:

1. The hadronic transverse momentum sum $p_{T,h}$ measures the missing transverse momentum with respect to the incoming particle direction in each event and is used as a main selection cut requiring

$$p_{T,h} = \sqrt{(\sum_i p_{x_i})^2 + (\sum_i p_{y_i})^2} > 25 \ \ \text{GeV} \ . \tag{5}$$

   The computation uses the event vertex position and energies and positions of LAr calorimeter cells (index i) of the hadronic final state. Neglecting particle masses the three components of the momentum vector are then defined by (p_x, p_y, p_z).

2. For both event types the CC trigger condition has to be fulfilled. For CC events this signal is derived from the LAr calorimeter trigger energies, for NC events it is evaluated from the same measurement after electron subtraction. To assign the events to a specific crossing of electron and proton bunches, a trigger signal from the proportional chambers is required.

3. A vertex is reconstructed from measured tracks. This vertex position has to be within a distance of 35 cm from the nominal interaction point along the beam axis.

4. High energy cosmic or proton beam related muons may cause large energy deposits in the calorimeter and thus fulfill the selection criteria. Based on the topology of these deposits and event timing with respect to the beam crossing background filters have been developed which remove these events efficiently [3].

The efficiency for these four selection criteria is determined from the initial NC sample. The selection efficiencies are found to be between 80% and 85% for the four processes with an uncertainty of 3%. All selection efficiencies depend only little on kinematic properties of the events. The final event statistics is given in Tab. 1.

The CC-candidate sample is subject to a visual inspection by which residual background from incoming muons and from misclassified NC events is identified and removed [3]. Photoproduction events $\gamma p \rightarrow hadrons$ in which the scattered electron remains undetected ($Q^2 \approx 0$) are a potential background for the CC sample if the hadronic final state is badly reconstructed due to particle losses in the beam pipe or resolution effects. This background has been estimated from data and was found to be less than 0.5% as described in [3, 12]. Therefore it has been neglected in further analysis here.

The total background rate for NC events is $2.0 \pm 0.6\%$ and has been statistically subtracted from the sample. The largest background contribution is due to γp events with many hadrons in the final state, one of which is misidentified as an electron. For some of these events the scattered electron is detected in the luminosity system of the H1 detector. From a study of these tagged events we find a background fraction of $1.4 \pm 0.6\%$ [12]. Events of the type $e^{\pm}p \rightarrow e^{\pm}e^{+}e^{-}X$ have been found by a visual inspection of the sample. They contribute an additional $0.3 \pm 0.2\%$ to the background. The background from incoming muons amounts to $0.3 \pm 0.1\%$.

4 Data Analysis

The final state kinematics is fully specified by two independent variables. Following the method proposed in [13] we use the transverse momentum sum $p_{T,h}$ (cf. eq. (5)) and the energy transfer y_h:

$$y_h = \sum_i (E_i - p_{z_i})/2E_e. \tag{6}$$

Here also particle masses are neglected and the summation is performed over all LAr calorimeter cells i of the hadronic final state.

For comparison to data and for studies of migration effects and unfolding we use a detailed detector simulation. The electroweak processes are generated by the DJANGO Monte Carlo program that includes QED radiative effects of order $\mathcal{O}(\alpha)$ [14] with proton parton densities of the MRSH parameterization [15]. The program makes use of the color dipole model as implemented in ARIADNE [16] for hadronization.

In Fig. 1 the measurements of $p_{T,h}$ and y_h are compared with the expectations from the simulation for the NC sample. The simulation agrees well with the measured distributions within the statistical errors.

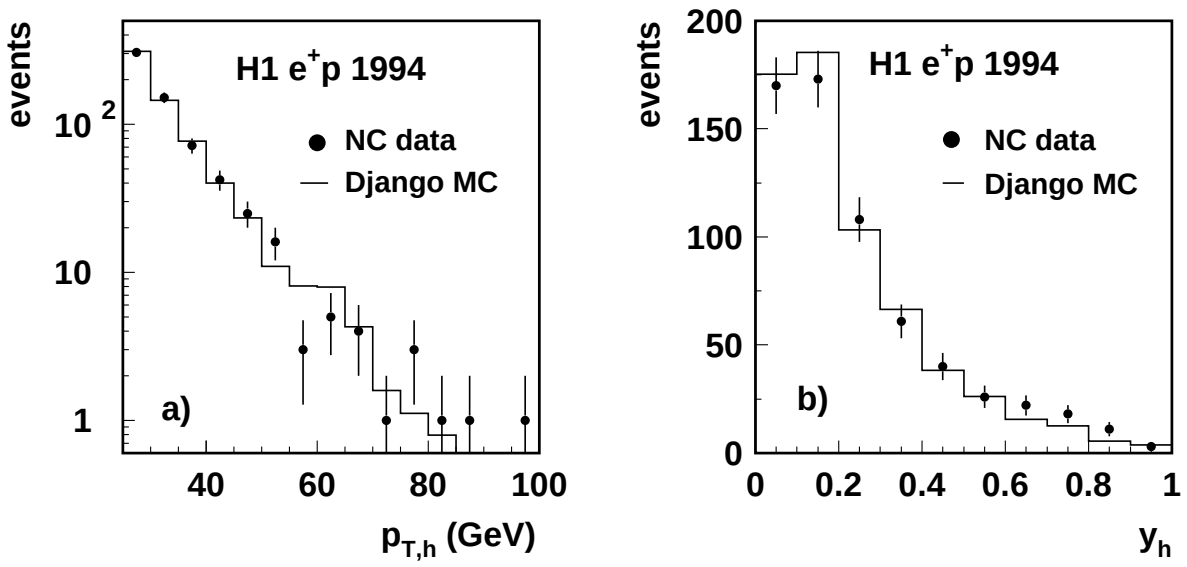

Figure 1: *Neutral current e^+p data (filled circles) are compared to a Monte Carlo (MC) simulation (histogram) normalized to the observed number of events. Shown is the transverse momentum sum $p_{T,h}$ of the hadronic final state is shown in (a) and y_h in (b) . For the data only statistical errors are given. The statistical errors from the MC simulation are negligible.*

The squared four momentum transfer Q^2 is related to $p_{T,h}^2$ and y_h by

$$Q_h^2 = \frac{p_{T,h}^2}{1 - y_h}. \tag{7}$$

The relative resolution for Q_h^2 is about 20%. For experimental cross checks the measurement of Q_e^2 by the scattered electron in NC events can be compared with Q_h^2 determined from the

hadronic final state. The lepton scattering angle ϑ_e and energy E'_e are used for calculating the kinematics with: $Q^2_e = 2E_eE'_e(1 + \cos(\vartheta_e))$. The Q^2_e measurement has a resolution $\Delta Q^2_e/Q^2_e \approx 3\%$. In Fig. 2 we compare the measured ratio Q^2_h/Q^2_e with the Monte Carlo simulation. The comparison shows that the hadronic measurement of the kinematics is well described by the simulation. The distribution is not centered around one due to losses in transverse momentum of the hadronic final state into the beam pipe.

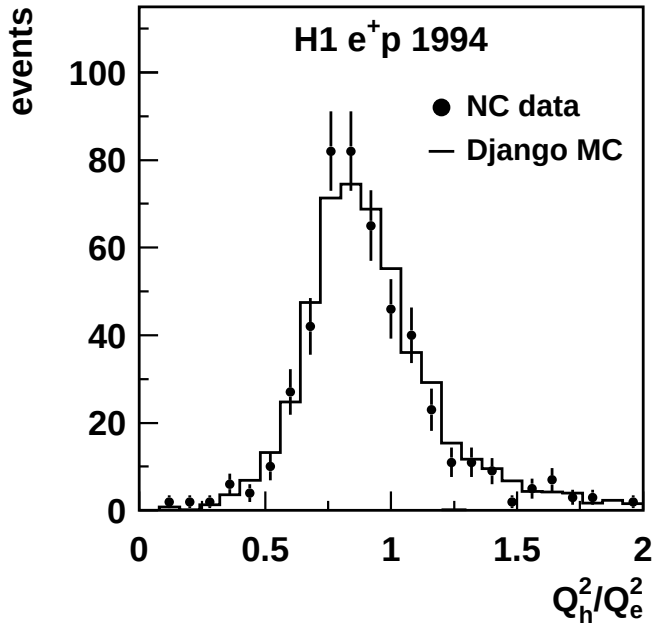

Figure 2: *The ratio of the squared four momentum transfer as determined from the hadronic final state Q^2_h and from the scattered electron Q^2_e for NC e^+p events compared to the Monte Carlo prediction. For the data only statistical errors are given. The statistical errors from the MC simulation are negligible.*

We apply a matrix unfolding technique [17] to determine the true Q^2 distribution from the measured Q^2_m distribution. The true squared four momentum Q^2 is defined by the outgoing lepton. For the unfolding we make use of the relation

$$\frac{d\sigma(Q^2_m)}{dQ^2_m} = \int dQ^2 A(Q^2_m, Q^2) \frac{d\sigma(Q^2)}{dQ^2}. \tag{8}$$

$A(Q^2_m, Q^2)$ is the detector response function averaged over the variable x. Consequently it has to be determined separately for the different processes under study. For finite Q^2 bins equation (8) can be converted into a sum:

$$\Delta\sigma(Q^2_m)_\mu = \sum_\nu T_{\mu\nu} \Delta\sigma(Q^2)_\nu \tag{9}$$

with bin indices μ and ν and the transfer matrix $T_{\mu\nu}$. The transfer matrix elements are determined by Monte Carlo simulation. They contain the transformation of the cut in $p_{T,h}$ into the corresponding experiment independent cut in the true p_T of the scattered lepton. The calculated transfer matrix is cross checked for NC data using the complementary information provided by the electron. The binning was chosen such (cf. Tab. 2), that the

majority (typically 60%) of the events are reconstructed into the original Q^2 bin. Inverting relation (9) and applying it to the measured binned distribution gives the true distribution together with its covariance matrix.

In binned distributions the information on individual events is lost. To exploit the full information on m_W contained in the shape of the CC Q^2 distribution and the total cross section we use the method of extended maximum likelihood [18]. The likelihood function is defined as:

$$L = \prod_{i=1}^{n} \frac{P_i(Q^2_m)}{\mathcal{N}} \cdot \frac{e^{-\mathcal{N}} \cdot \mathcal{N}^n}{n!} \tag{10}$$

where i runs over n individual events. For an event i the distribution $P_i(Q^2_m)$ in four momentum Q^2_m is given by the convolution of the differential cross section $d\sigma(Q^2, m_W)/dQ^2$ and the detector response function $A(Q^2_m, Q^2)$ (cf. eq. (8)). The predicted number of events for a propagator mass m_W and an integrated luminosity $\mathcal{L}$ is $\mathcal{N} = \mathcal{L} \int P(Q^2_m) dQ^2_m$. The propagator mass is then extracted from the data by maximizing the likelihood function.

5 Results

In Fig. 3 and Tab. 1 we present the result of the unfolding of the Q^2-differential cross sections for the $e^{\pm}p$ data for NC and CC for $p_T > 25$ GeV. The theoretical prediction was obtained with the HERACLES [19] generator using the MRSA′ [15] proton parton densities. The uncertainty of the prediction is about 4% due to the imperfect knowledge of the parton densities. Note that the data are not corrected for radiative effects. Born cross sections can be obtained using $d\sigma_{Born}/dQ^2 = d\sigma/dQ^2(1 + \delta_{Born})$ (cf. Tab. 2). A factor c_{p_T} which can be used additionally to correct the measured cross section to the full phase space $d\sigma/dQ^2(p_T > 0 \text{ GeV}^2) = c_{p_T} d\sigma/dQ^2(p_T > 25 \text{ GeV}^2)$ is given in Tab. 2. The error on c_{p_T} accounts for uncertainties in the structure functions. Results are given at fixed Q^2 values, therefore the measured bin averaged cross section has been corrected by the factor $c_{bin} = \frac{d\sigma^{theor.}(Q^2)}{dQ^2} / \frac{\Delta\sigma^{theor.}}{\Delta Q^2}$ which is given in Tab. 2. Differences in center of mass energy for different running periods are taken into account and the results are given for $s = 90200$ GeV^2.

Agreement with the Standard Model prediction is observed. Our result for NC is also in agreement with the differential cross section measurements based on essentially the same data using the electron variables presented in [5] with slightly different selection criteria. Above $Q^2 = 5000$ GeV^2 the cross sections for neutral and charged current processes are of comparable size. For the e^+p data the charged current cross section stays below the neutral current cross section over the whole Q^2 range, due to the different $y-$dependence of the quark contributions to the cross section (cf. eq. (3,4), [3]).

The CC cross section errors are dominated by the statistical errors whereas for the NC samples the main contribution to the errors comes from the uncertainty in the hadronic energy scale. Other sources of systematic errors are uncertainties in the determination of the trigger and selection efficiencies as well as the luminosity measurement.

For the neutral current cross section we show in Fig. 3 the Standard Model expectation for γ, Z^0 exchange and assuming photon exchange only. This illustrates that the present integrated luminosity does not yet allow the distinction between the pure photon exchange and the total electroweak cross section in NC reactions.

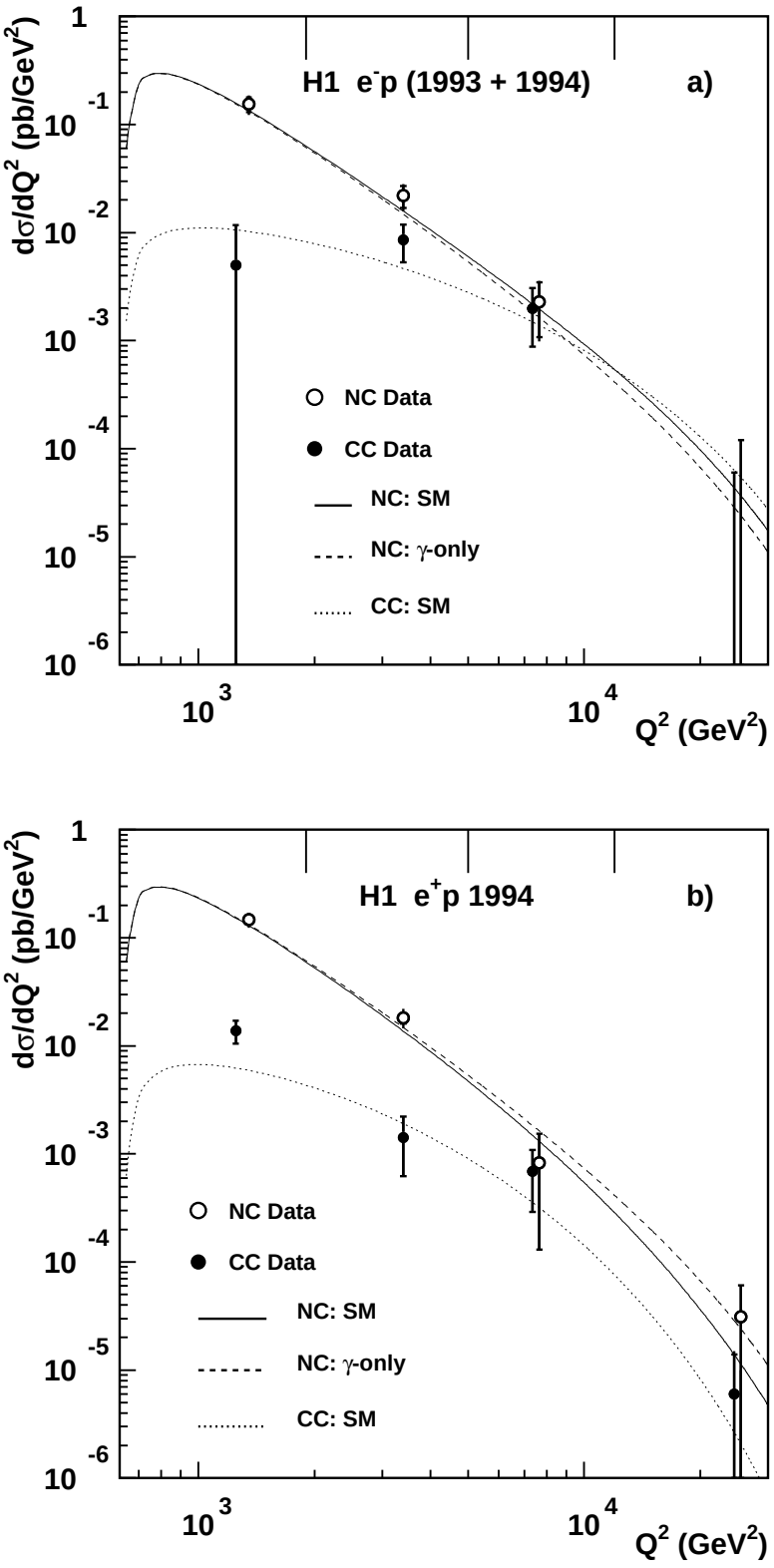

Figure 3: *The unfolded differential cross sections $d\sigma/dQ^2$ are shown for charged and neutral current interactions with $p_T > 25$ GeV for e^-p collisions in* a) *and for e^+p collisions in* b)*. The inner error bars contain statistical, the full error bars include also the systematic errors added in quadrature. Boundaries of each bin are denoted by the vertical bars on the top of the plots. The solid lines indicate the Standard Model predictions for neutral current interactions and the dotted lines for charged current interactions. Dashed lines show the prediction for NC from photon exchange alone.*

		e^-p		e^+p	
$\frac{Q^2}{GeV^2}$		NC	CC	NC	CC
1250	events	105	6	370	26
	$\frac{d\sigma/dQ^2}{fb/GeV^2}$	$155 \pm 24 \pm 21$	$5.0 \pm 6.7 \pm 0.9$	$146 \pm 12 \pm 20$	$13.7 \pm 3.3 \pm 0.7$
3400	events	42	14	133	13
	$\frac{d\sigma/dQ^2}{fb/GeV^2}$	$21.9 \pm 5.0 \pm 3.6$	$8.6 \pm 3.3 \pm 0.7$	$18.2 \pm 2.2 \pm 3.0$	$1.4 \pm 0.8 \pm 0.2$
7500	events	6	5	16	7
	$\frac{d\sigma/dQ^2}{fb/GeV^2}$	$2.3 \pm 1.2 \pm 0.4$	$2.0 \pm 1.1 \pm 0.3$	$0.8 \pm 0.7 \pm 0.2$	$0.7 \pm 0.4 \pm 0.1$
25000	events	0	0	2	1
	$\frac{d\sigma/dQ^2}{fb/GeV^2}$	$0.00 \pm 0.12 \pm 0.01$	$0.00 \pm 0.06 \pm 0.04$	$0.03 \pm 0.03 \pm 0.01$	$0.006 \pm 0.008 \pm 0.003$
total	events	153	25	521	47
	σ/pb	$331 \pm 27 \pm 47$	$46 \pm 9 \pm 3$	$299 \pm 13 \pm 42$	$23 \pm 3 \pm 2$
	σ_{SM}/pb	294 ± 12	40.7 ± 1.6	276 ± 11	15.6 ± 0.6

Table 1: *Event statistics, differential, and total cross sections for $p_T > 25$ GeV are listed for NC and CC processes in e^+p and e^-p running. The first error is of statistical nature and obtained from the diagonal element of the covariance matrix, the second accounts for systematic uncertainties. The total cross sections are compared with the Standard Model prediction for $m_W = 80.2$ GeV and using the MRSA′ parameterization for the proton parton densities.*

From the CC sample we obtain using the extended maximum likelihood fit a propagator mass of

$$m_W(e^-p) = 78\ ^{+11}_{-9}\ ^{+4}_{-3}\ \text{GeV}\ , \qquad m_W(e^+p) = 97\ ^{+18}_{-15}\ ^{+5}_{-10}\ \text{GeV},$$

where the first errors are of statistical and the second of systematic origin. The statistical uncertainties reflect the different sensitivities of the e^+p and e^-p cross sections to the propagator mass. The main source of systematic errors is the hadronic energy scale. The masses for both charge states are compatible and a combined fit results in

$$m_W = 84\ ^{+9}_{-6}\ ^{+5}_{-4}\ \text{GeV}.$$

Exploiting the Q^2 shape alone gives a consistent but less precise value for the propagator mass.

The shape and cross section analysis exhibits that both charged current processes are consistent with the exchange of a W boson which has equal mass for both charge states. This confirms previous results from HERA on the W-mass [2, 3, 4] with improved precision. In addition the mass of the intermediate W boson is in agreement with the mass determined from direct production of W bosons at $p\bar{p}$-colliders [20].

In this analysis we use a larger angular coverage for the tracks entering the vertex reconstruction compared to our previous analysis where the polar angular acceptance started at 15° [3]. On the basis of this extended acceptance we update the total CC cross sections

published in [3]. These cross sections as well as the ones for NC are collected in Tab. 1. The Standard Model expectations are calculated as before using the HERACLES generator, where the error on the expectation originates in the choice of the proton structure function.

We present also the ratios of total NC and CC cross sections $R = \sigma_{NC}/\sigma_{CC}$. Due to the same treatment of neutral and charged current events many systematic errors cancel in this ratio. For $p_T > 25$ GeV we obtain

$$R^+(e^+p) = 12.8 \pm 2.0 \pm 1.0 \qquad R^-(e^-p) = 7.2 \pm 1.6 \pm 0.7. \tag{11}$$

The result for R^- is in good agreement with the theoretical prediction of $R^-_{SM} = 7.2 \pm 0.1$. We observe a two standard deviation discrepancy for R^+ from the prediction $R^+_{SM} = 17.7 \pm 0.9$.

The residual systematic uncertainty is still caused by the hadronic energy scale due to the different cross section slope of NC and CC near the selection cut of $p_{T,h} = 25$ GeV. Selecting only events above $Q^2 = 5000$ GeV^2, where the cross section slopes are nearly identical reduces the systematic uncertainty further. For such a cut we obtain $R^+ = 2.0 \pm 1.4 \pm 0.07$ and $R^- = 1.4 \pm 0.8 \pm 0.05$, while the expected values are $R^+ = 4.17$ and $R^- = 1.34$. With higher integrated luminosity these cross section ratios will be sensitive probes for precision tests of the Standard Model [21].

			e^-p		e^+p	
$\frac{Q^2}{GeV^2}$	Q^2 range		NC	CC	NC	CC
1250	625–1500	c_{bin}	0.956	1.191	0.950	1.213
		δ_{Born}	-0.02 ± 0.01	0.06 ± 0.02	-0.02 ± 0.01	0.06 ± 0.02
		c_{p_T}	1.30 ± 0.01	1.29 ± 0.01	1.30 ± 0.01	1.34 ± 0.01
3400	1500–5000	c_{bin}	0.703	0.990	0.674	0.939
		δ_{Born}	-0.08 ± 0.01	0.04 ± 0.02	-0.09 ± 0.01	0.04 ± 0.02
		c_{p_T}	1.10 ± 0.01	1.10 ± 0.01	1.10 ± 0.01	1.11 ± 0.01
7500	5000–12000	c_{bin}	0.949	1.129	0.894	1.099
		δ_{Born}	-0.09 ± 0.01	0.02 ± 0.02	-0.12 ± 0.01	0.02 ± 0.02
		c_{p_T}	1.06 ± 0.01	1.06 ± 0.01	1.05 ± 0.01	1.07 ± 0.01
25000	12000–s	c_{bin}	1.142	1.47	0.729	0.667
		δ_{Born}	-0.07 ± 0.01	-0.02 ± 0.02	-0.19 ± 0.01	-0.02 ± 0.02
		c_{p_T}	1.04 ± 0.01	1.04 ± 0.01	1.03 ± 0.01	1.04 ± 0.01

Table 2: *For each Q^2 bin the bin boundaries, the applied correction factor for the finite bin size c_{bin} and the correction factors to obtain a Born cross section δ_{Born} and to correct for the full phase space c_{p_T} are given.*

6 Conclusion

The Q^2 dependence of the neutral and charged current processes have been measured for e^- and e^+ beams colliding with protons for transverse momenta of the scattered lepton above 25 GeV. The analysis is based on the properties of the hadronic final state in both cases. The differential cross sections, as well as the total cross sections and their ratios are in agreement with the Standard Model expectations. At large momentum transfers $Q^2 > 5000$ GeV^2 we observe that the weak and electroweak forces have the same strength. The propagator masses measured in charged current scattering are consistent with being the same for both charges. The average is $m_W = 84\ ^{+10}_{-7}$ GeV and is consistent with the on-shell measurement of the W boson mass.

Acknowledgment

We are grateful to the HERA machine group whose outstanding efforts made this experiment possible. The immense effort of the engineers and technicians who constructed and maintained the detector is appreciated. We thank the funding agencies for financial support. We acknowledge the support of the DESY technical staff and wish to thank the DESY directorate for the hospitality extended to the non-DESY members of the collaboration. We thank H. Spiesberger for discussions concerning radiative corrections and help with the theoretical calculations.

References

[1] G.Ingelman et al., Proceedings of the HERA Workshop, Hamburg, Vol. 1 (1987) 3.

[2] H1 Collaboration, T. Ahmed et al., Phys. Lett. B324 (1994) 241.

[3] H1 Collaboration, S. Aid et al., Z. Phys. C67 (1995) 565.

[4] ZEUS Collaboration, M. Derrick et al., Phys. Rev. Lett. 75(1995)1006.

[5] H1 Collaboration, S. Aid et al., Phys. Lett. B353 (1995) 578.

[6] H1 Collaboration, S. Aid et al., *A Measurement and QCD Analysis of the Proton Structure Function $F_2(x, Q^2)$ at HERA,* DESY 96-039.

[7] H1 Collaboration, I. Abt et al., *The H1 detector at HERA*, DESY Preprint 93-103 (1993).

[8] H1 Calorimeter Group: B. Andrieu et al., Nucl. Instr. and Meth. A336 (1993), 460.

[9] H1 Calorimeter Group, B. Andrieu et al., Nucl. Instr. and Meth. A336 (1993), 499 ; ibid. A350 (1994) 57.

[10] M. Flieser, Ph.D. thesis TU Munich, Fakultät für Physik, 1996, in litt.

[11] H1 Collaboration, T. Ahmed et al., Z. Phys. C66 (1995) 529.

[12] A. Schöning, Ph.D. thesis, University of Hamburg, 1996, in litt.

[13] F. Jacquet and A. Blondel, Proceedings of the "Study for an ep Facility in Europe" (1979) 391.

[14] G.A. Schuler and H. Spiesberger, DJANGO: Proceedings of the Workshop "Physics at HERA", Hamburg, Vol. 3 (1991) 1419.

[15] A.D. Martin, W.J. Stirling and R.G. Roberts, Phys. Rev. D50 (1994) 6734, Phys. Rev. D51 (1995) 4756.

[16] L. Lönnblad, Comm. Phys. Comm. 71 (1992) 433.

[17] G. Zech, *Comparing Statistical Data to Monte Carlo Simulation: Parameter Fitting and Unfolding,* DESY-95-113.

[18] R. Barlow, Nucl. Inst. and Meth. A297 (1990) 496.

[19] A. Kwiatkowski, H. Spiesberger and H.-J. Möhring, Comp. Phys. Comm. 69 (1992) 155.

[20] Particle Data Group, Phys. Rev. D50 (1994) 1191.

[21] V. Brisson et al., Proceedings of the Workshop "Physics at HERA", Hamburg, Vol. 2 (1991) 947.